AGU PUBLICATIONS

Paleoceanography

RESEARCH ARTICLE
10.1002/2016PA003030

Key Points:
- Multiproxy records of Makassar Strait hydrology over the past 14 ka
- Slowdown of Indonesian Throughflow and drying of Borneo during Younger Dryas
- Latitudinal displacement of ITCZ controlled Makassar Strait surface hydrology

Supporting Information:
- Supporting Information S1
- Data Set S1

Correspondence to:
M. Hendrizan,
hendrizan@geotek.lipi.go.id;
m_hendrizan@yahoo.com

Citation:
Hendrizan, M., Kuhnt, W., & Holbourn, A. (2017). Variability of Indonesian Throughflow and Borneo runoff during the last 14 kyr. *Paleoceanography, 32*, 1054–1069. https://doi.org/10.1002/2016PA003030

Received 30 AUG 2016
Accepted 27 SEP 2017
Accepted article online 5 OCT 2017
Published online 26 OCT 2017

Variability of Indonesian Throughflow and Borneo Runoff During the Last 14 kyr

Marfasran Hendrizan[1,2], Wolfgang Kuhnt[1], and Ann Holbourn[1]

[1]Institute of Geosciences, Christian-Albrecht-University, Kiel, Germany, [2]Research Centre for Geotechnology, Indonesian Institute of Sciences, Bandung, Indonesia

Abstract We present a high-resolution (~20 to 100 years temporal resolution) reconstruction of hydrological changes in the Makassar Strait over the last 14 kyr from Core SO217-18517 retrieved off the Mahakam Delta (1°32.198′S, 117°33.756′E; 698 m water depth) during the SO217 Makassar-Java Cruise. Sea surface temperatures, based on Mg/Ca of *Globigerinoides ruber* and alkenone $U^{K'}_{37}$, and seawater $\delta^{18}O$ reconstructions, based on *G. ruber* $\delta^{18}O$ and Mg/Ca, in combination with sortable silt grain size measurements and X-ray fluorescence (XRF) core scanner derived elemental data provide evidence for increased precipitation during the Bølling-Allerød (BA) and early Holocene and for warmer and more saline surface waters and a decrease in the intensity of the Indonesian Throughflow (ITF) during the Younger Dryas (YD). XRF derived Log (Zr/Rb) records, sortable silt data and increased sedimentation rates indicate decreased winnowing, interpreted as a slowdown of the ITF thermocline flow during the YD. We attribute this decline in ITF intensity to slowdown of the Atlantic meridional overturning circulation during the YD. We suggest that changes in Makassar Strait surface hydrology during this interval of Northern Hemisphere cooling and Southern Hemisphere warming were related to a southward displacement of the Intertropical Convergence Zone.

1. Introduction

The variability of the Indonesian Throughflow (ITF) during the last glacial cycle has been related to major cooling events in the Northern Hemisphere and associated southward displacement of the Intertropical Convergence Zone (ITCZ) (e.g., Holbourn et al., 2011; Mohtadi et al., 2011; Zuraida et al., 2009). Episodes of intense cooling and slowdown or even collapse of the Atlantic meridional overturning circulation (AMOC) during Heinrich Events (Ganopolski & Rahmstorf, 2001; Broecker, 2003; Piotrowski et al., 2005) exhibit striking similarities to the Younger Dryas (YD) cooling event at the end of the last deglaciation (Denton et al., 2010), which has even been referred to Heinrich 0 Event by some authors (Andrews et al., 1995; Kirby, 1998). A number of studies suggested that the YD climate change was probably related to a reduction in the AMOC (e.g., Stouffer et al., 2006), resulting in an increase of the Southern Ocean-derived deep-water volume in the North Atlantic (Boyle & Keigwin, 1987) and a reduction of the North Atlantic deep-water export (Henry et al., 2016; McManus et al., 2004). Numerical models predicted that a slowdown in the global thermohaline circulation results in a weakening of the ITF, which in turn reduces the southward directed warm Leeuwin Current off Western Australia and the fresh and cool thermocline flow feeding the South Equatorial Current (De Deckker et al., 2003; Gordon, 2005). Temperature and $\delta^{18}O$ of seawater ($\delta^{18}O_{sw}$) reconstructions from Core MD01-2378 in the Timor Sea indicated warm and salty upper thermocline water during Heinrich events (HEs), related to weakening of the ITF through the Timor Strait (Zuraida et al., 2009). However, no evidence for ITF variability during HEs or the YD is so far available from the upstream path of the ITF in the Makassar Strait due to the scarcity of continuous, high-resolution records from thermocline water depths.

The first objective of this study was to address the lack of information on past ITF variability within the Makassar Strait. Therefore, Core SO217-18517 (1°32.198′S, 117°33.756′E; 698 m water depth) was retrieved ~90 km off Borneo (Figures 1a and S1 in the supporting information) on a submarine high, offshore the southeast distributary of the Mahakam River Delta. Today, the sea floor at this location below the main flow path of the ITF is still influenced by the lower thermocline ITF with relatively low annual average southward flow speed of ~0.1 m/s but seasonal maxima of ~0.3 m/s (Gordon et al., 2008). Winnowing of fine-grained particles occurs seasonally and during periods of enhanced ITF such as during strong La Niña events. Significantly higher flow speeds in the upper thermocline (up to 0.6 m/s annual average and seasonal maxima of 0.9 m/s (Gordon et al., 2008) additionally promote lateral advection of clay particles from more northerly

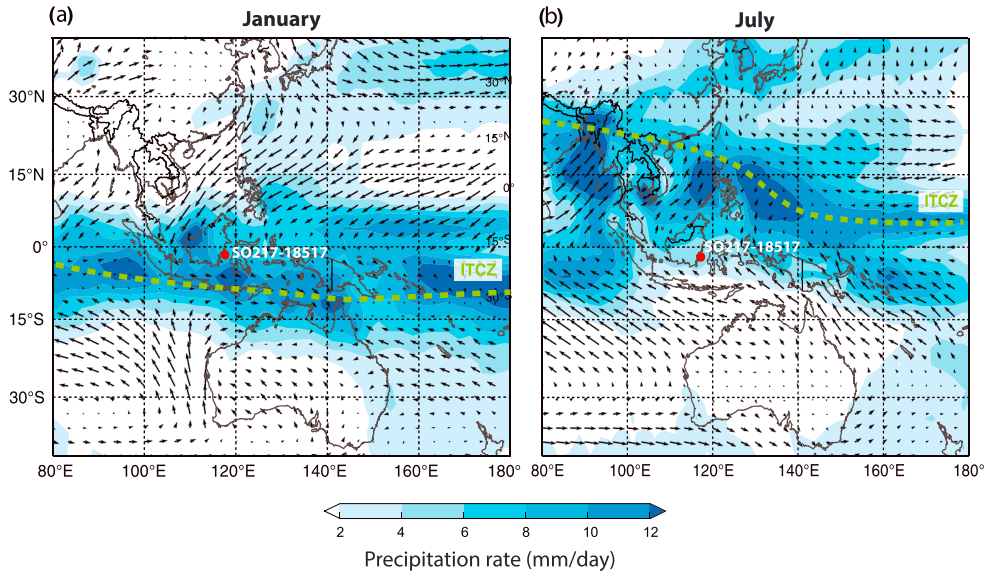

Figure 1. Seasonal changes in regional wind patterns associated with latitudinal displacement of ITCZ. (a) The ITCZ position occurs in the south during January; (b) the ITCZ in the north during July. Wind data are derived from the National Center for Environmental Prediction (NCEP) reanalysis project, available at http://www.esrl.noaa.gov/psd/. Precipitation data are from Xie and Arkin (1997): Climate Prediction Center Merged Analysis of Precipitation (CMAP) precipitation estimates during 1981–2010, available at http://iridl.ldeo.columbia.edu. Green dashed line indicates mean monthly position of ITCZ, following Waliser and Gautier (1993) and Fraser et al. (2014).

sources into the central and southern part of the Makassar Strait (Dekov et al., 1999; Eisma et al., 1989). Thus, the terrigenous particles accumulating at Site SO217-18517 may also include suspended material from northern Borneo rivers with catchment areas in different climatic and geologic regions (Aldrian & Susanto, 2003; Hall & Nichols, 2002).

High concentrations of suspended sediment, in the range >2 mg/dm^3, occur off the Mahakam River mouth (Dekov et al., 1999; Eisma et al., 1989). The high terrigenous input from the Mahakam River plume maintains a relatively low carbonate content in sediments around the Mahakam River outflow in contrast to other locations in the Makassar Strait and Flores Sea, which are not affected by the high terrigenous flux from eastern Borneo (Dekov et al., 1999). Eastern Borneo Rivers have among the highest yields of suspended matter in the world, due to a combination of their locations in an active tectonic area, steep mountains, and torrential seasonal rainfall (Milliman & Farnsworth, 2011; Milliman et al., 1999). In particular, the Mahakam River, which is one of the largest rivers on Borneo, discharges 3.6 Mt of suspended load per year into the Makassar Strait, where it has built up a large fan-shaped delta (Eisma et al., 1989; Milliman & Farnsworth, 2011). A characteristic low salinity plume indicates preferential transport of Mahakam suspended load toward the SE into the center of the Makassar Strait (Dekov et al., 1999; Eisma et al., 1989) with the position of Site SO217-18517 approximately in the center of this plume.

A second objective of this study was to closely monitor runoff and salinity changes at the front of the Mahakam Delta over the last deglaciation and Holocene. The reconstruction of hydrological changes related to tropical convective activity over the Indonesian archipelago on millennial timescale remains a challenge due to the scarcity of high-resolution precipitation records from the maritime continent of Indonesia. The few available records from North Australia, South Java, Flores (e.g., Griffiths et al., 2009; Kuhnt et al., 2015; Mohtadi et al., 2011) show contrasting evidence of a dry HE1 and YD in Java and a wet HE1 and YD in the Flores Sea and NW Australia. These records agree to some extent with the recent hypothesis of enhanced tropical convection and intensified Walker circulation during global (tropical) cooling (DiNezio et al., 2011). These modeling studies suggested that seasonal rainfall increases locally during colder periods in the areas of the South China Sea, Celebes Sea, and Makassar Strait, where convection is considerably enhanced (DiNezio et al., 2011). However, this hypothesis does not account for the sharp regional contrast between records and needs to be tested in high-resolution sedimentary archives that allow to differentiate variations in the salinity related δ^{18}O of seawater and continental runoff.

The location of Site SO217-18517 and the adjacent catchment and delta of the Mahakam River are characterized by a tropical climate with significant rainfall throughout the year in the Samarinda region (supporting information Figure S2). The rainfall averages ~2,100 mm/yr with ~120 mm even in the driest month and a relatively small difference of ~100 mm between the wettest (March–April) and the driest months (August–September). Today, the intensity of convective precipitation at this location is related to the seasonal migration of the ITCZ, which passes over the area twice: in January–April during its northward swing and in September–December during its southward displacement (supporting information Figures S2 and S3). However, the seasonality of the ITCZ migration was substantially altered over the last deglaciation and Holocene. Seasonal insolation, which drives the ITCZ position over the Mahakam Delta (1°S), differed from the present day insolation maximum in January (driving the ITCZ northward). The early to middle Holocene period was characterized by a dominant September insolation maximum (driving the ITCZ southward), whereas a strong January maximum occurred at the end of HE1 (15 ka) (supporting information Figure S3). These changes in the seasonality of insolation may have had significant impact on local hydrologic patterns and need to be taken into account in reconstructions of deglacial hydrology.

To fulfill these two main objectives, we generated sea surface temperature (SST) estimates from Mg/Ca of *Globigerinoides ruber* and alkenone $U^{K'}_{37}$, $\delta^{18}O_{sw}$ records from $\delta^{18}O$ and Mg/Ca of *G. ruber*, X-ray fluorescence (XRF) core scanning data related to sediment discharge and winnowing, as well as bottom current intensity estimates based on grain size (sortable silt) in Core SO217-18517. Our aims are to decipher changes in ITF bottom water flow intensity in relation to surface hydrologic changes in the central Makassar Strait off East Borneo over the last termination and Holocene. These new data will contribute to a better understanding of the temporal and spatial evolution of tropical precipitation over central Indonesia and associated variations in ITF intensity during the last deglaciation and will, thus, help elucidate potential relations between tropical climate variability, global circulation patterns, and high-latitude climate change.

2. Material and Methods

Core SO217-18517 was retrieved with a Split-Piston Corer during the SO217 Makassar-Java (MAJA) Cruise aboard R/V *Sonne* in July–August 2011 (Kuhnt et al., 2011). The coring position was located at 1°32.198′S, 117°33.756′E in 698 m water depth, offshore the southeast distributary of the Mahakam River Delta, which discharges large amounts of terrigenous sediment into the Makassar Strait (Dekov et al., 1999; Eisma et al., 1989; Saller et al., 2004; Storms et al., 2005). The coring site was chosen on a topographic high to reduce the likelihood of turbidite deposition (Kuhnt et al., 2011). Core SO217-18517 is 14.27 m long and mainly consists of homogenous dark green/gray fine-grained clay (supporting information Figure S4).

2.1. Sampling Strategy

Core SO217-18517 was initially sampled at 10 cm intervals (1 cm thick half slices) equivalent to ~100 years time resolution in the upper part of the core (middle to late Holocene). The lower part of the core (deglacial to early Holocene) was subsequently sampled at 2 cm intervals (~20 years time resolution). A total of 375 and 345 samples were analyzed for planktonic foraminiferal stable isotopes and Mg/Ca, respectively. Stable isotope and Mg/Ca preparation followed the procedure detailed in previous studies in this region (Bolliet et al., 2011; Zuraida et al., 2009). In rare samples, where the number of foraminiferal tests was low, we included foraminifers from the adjacent 1 cm thick half slice.

2.2. X-Ray Fluorescence Core Scanning

Technical details and practical operation of the XRF core scanner are described in Richter et al. (2006), and metadata on scanning settings are provided in the supporting information. Single element areal counts per second from the XRF measurements were normalized using log ratios to reduce volume effects related to the abundance of other elements (Weltje & Tjallingii, 2008).

To estimate changes in grain density (related to grain size changes), we used the log normalized Zr/Rb. Zr is enriched in heavy minerals (zircon) and associated with a coarser grained fraction, whereas Rb is enriched in light clay minerals and characteristic of fine grain sizes (Dypvik & Harris, 2001; Kylander et al., 2011; Schneider et al., 1997). Thus, the normalized Zr/Rb as an estimate of coarse and fine-grained detritus in the sediment can serve as a proxy of current energy (Liu et al., 2002; Lo Giudice Cappelli et al., 2016; Schulte & Speijer, 2009). We used the log ratio of potassium (K) and titanium (Ti) as a proxy of riverine sediment discharge (Kujau et al.,

2010), based on the assumption that K dominates in the fine-grained fluvial sediment discharge from the Mahakam River, since K weight percentages in surface samples from the Mahakam River reach relatively high values of 2.4–2.6% in the clay fraction (<2 μm) (Liu et al., 2012). Bulk sediment (<63 μm) from this area, which is more representative of the total runoff (including aeolian, small rivers, and along-slope basinal transport), is characterized by lower K content (1.3 and 1.6%) and, thus, lower K/Ti log ratios. K/Ti values are usually elevated in clay-rich sediments that have a relatively high illite content, derived from source areas with common physical weathering such as the mountainous catchment areas of the Mahakam River in the highland of Central Borneo.

2.3. Stable Isotopes

For $\delta^{18}O$ analysis, approximately 10 tests of *G. ruber* were picked from the size fraction 315–250 μm at 10 cm intervals over the interval 9 to 0 ka. Between 14 and 9 ka, sample spacing was decreased to 2 cm. All tests were gently crushed into large fragments, agitated in ethanol for 1 s in an ultrasonic bath, decanted, and dried at 40°C. $\delta^{18}O$ was measured with a Finnigan MAT 253 mass spectrometer (Carbo-Kiel Device (Type IV) for automated CO_2 preparation from carbonate samples for stable isotopic analysis) at the Leibniz Laboratory, Christian-Albrechts-University, Kiel. The samples were reacted by individual acid addition (99% H_3PO_4 at 75°C). Standard external error is better than ±0.0 9‰ for $\delta^{18}O$, as documented by the performance of international and laboratory-internal carbonate standard materials.

2.4. Mg/Ca Measurements

Thirty well-preserved tests of *G. ruber* were selected from the size fraction 315–250 μm, weighed with an ultraprecision balance (Sartorius ME5 OCE), gently crushed between two glass plates to expose the inner chamber walls and put into vials for cleaning. Cleaning procedures for removing contaminant phases were applied with oxidative and reductive steps following the methods described in Martin and Lea (2002). A freshly prepared subboiled HNO_3 was used, and all work was conducted on a class 100 clean bench. The dissolved samples were analyzed on a radial viewing simultaneous ICP-OES (Spectro Ciros SOP CCD, Spectro Analytical Instruments, Germany) at the Institute of Geosciences, Christian-Albrechts-University Kiel, applying an intensity calibration method (Villiers et al., 2002) and bracketing standards. The external error is 0.1% rel. (1 sigma) for Mg/Ca. Matrix effects caused by the easily ionizable element Ca were investigated and found to be negligible. Samples with a recovery in Ca concentration below 20% were rejected. Fe/Ca, Al/Ca, and Mn/Ca were additionally monitored to test cleaning efficiency and samples showing a significant correlation between Fe/Ca, Al/Ca, Mn/Ca, and Mg/Ca values were excluded, following Schmidt et al. (2004).

Foraminiferal Mg/Ca were converted into temperature using the equation of Anand et al. (2003), providing an accuracy of ±1.2°C in estimating calcification temperatures (*T* in °C):

$$\mathrm{Mg/Ca} = 0.38 \ \exp 0.09\, T \text{ for } \textit{Globigerinoides ruber}$$

We applied no correction for the reductive step included in the cleaning protocol, which generally results in a small decrease in Mg/Ca leading to temperature underestimation of up to ~1°C (Barker et al., 2003).

2.5. $U^{K'}_{37}$ SST Estimates

Sea surface temperatures were estimated at 10 cm intervals using the alkenone-based $U^{K'}_{37}$ proxy over the 14–7 ka interval and at 50 cm intervals over the 7–0 ka interval. Alkenones were extracted from 1 g of homogenized bulk sediments and analyzed with double column gas chromatography at the Institute of Geosciences, Christian-Albrechts-University Kiel, following the procedure of Rincón-Martínez et al. (2010). The calibration of $U^{K'}_{37}$ (ratio of 0.937 to 0.987) followed the temperature reconstruction of Muller et al. (1998), which has been developed for temperature 0–29°C in core tops with a global distribution using the equation:

$$\mathrm{SST}\ (°\mathrm{C}) = \left(U^{k'}{}_{37} - 0.044\right)/0.033$$

Toward the limits of alkenone saturation at ~29°C, the relationship between temperature and the $U^{K'}_{37}$ index becomes less reliable. It diverges from the linear relationship, which is the base of the calibration by Muller et al. (1998), and tends to display a sigmoidal relationship (Conte et al., 2006; Sonzogni et al., 1997). This is

reflected in the lower variability of SST in the Holocene part of the SO217-18517 record, when SST fluctuate around 28.5°C, but does not affect the temperature reconstruction during the glacial termination, when alkenone based SST consistently remains well below 28.5°.

2.6. Radiocarbon Dating and Age Model

For accelerator mass spectrometry (AMS) ^{14}C dating, approximately 6 mg of well-preserved pteropod shells were picked from the >355 μm size fractions, where sufficient numbers of shells were found. In instances of low abundance, mixed planktonic foraminifers consisting of *G. ruber*, *Globigerinoides sacculifer*, *Globigerinoides trilobus* were analyzed. AMS^{14}C analysis was performed at the Leibniz Laboratory, Christian-Albrechts-University, Kiel. One replicate measurement using a sample with mixed planktonic foraminifers consisting of *G. ruber*, *G. sacculifer*, and *G. trilobus* (KIA 47980) and a sample with pteropods (KIA 47981) at 1,237 cm (section 14, 10–11 cm) indicates an age difference of 150 years (conventional age). We did not correct for the slightly older age of pteropods, since this age difference is close to the combined standard error. We applied a 400 years reservoir age correction before conversion to calendar ages, consistent with other studies in this region (Linsley et al., 2010; Visser et al., 2003). Conventional ages were converted to calendar ages following the protocol established by Fairbanks et al. (2005).

The age model is constrained by eight AMS ^{14}C dates based on planktonic foraminifers and pteropods. An interpolated curve was fitted through the eight AMS ^{14}C tie points using a Stineman function (smooth function in Kaleidagraph). The output of the function has a geometric weight applied to the current point and ±10% of the data range. The resulting smoothed curve was, then, sampled at relevant intervals for each data set.

2.7. Paleosalinity Reconstruction From $\delta^{18}O_{sw}$

We calculated surface seawater δ^{18}O ($\delta^{18}O_{sw}$ versus V-SMOW) from paired Mg/Ca and δ^{18}O measurements of *G. ruber*. For this, we used the equation of Bemis et al. (1998):

$$\delta^{18}O_{sw} = 0.27 + \left(T\ (°C) - 16.5 + 4.8 \times \delta^{18}O\ (V - PDB)\right)/4.8$$

Substituting the lower resolution $U^{K'}_{37}$ temperature estimates does not affect the $\delta^{18}O_{sw}$ reconstruction (supporting information Figure S8). As the equation deducts the effect of temperature during fractionation of oxygen isotopes, the calculated $\delta^{18}O_{sw}$ is mainly related to continental ice volume and local $\delta^{18}O_{sw}$ fluctuations associated with surface salinities. Therefore, to remove the ice volume effect in order to estimate surface salinities, we additionally applied an ice volume correction based on the effect of past sea level changes on $\delta^{18}O_{sw}$ of the global ocean (Sarnthein et al., 2011).

The relation between $\delta^{18}O_{sw}$ and salinity exhibits strong regional variability (Fairbanks et al., 1997; Morimoto et al., 2002). A regression of δ^{18}O versus salinity in the western Pacific warm pool (WPWP) indicates a slope of 0.42 (Morimoto et al., 2002), while samples from corals in the equatorial western and central Pacific Ocean exhibit a slope of only 0.27 (Fairbanks et al., 1997). These differences are related to different evaporation-precipitation conditions and resulting δ^{18}O of precipitation in each region. Additionally, salinity measurements in the Makassar Strait indicated that our coring site is influenced by the plume from the Mahakam River (supporting information Figure S1), which disperses over an area of ~400 km to the southeast of the Mahakam Delta with salinity values ranging from 33 to 34 practical salinity unit (psu) (Dekov et al., 1999; Eisma et al., 1989; Storms et al., 2005).

2.8. Grain Size Analysis

Sediment grain sizes were measured with a Beckman Coulter *LS* 13 320 laser diffraction particle size analyzer at the Institute of Geosciences, Christian-Albrecht-University, Kiel. The device allocates particles in 116 size classes between 0.041 μm and 1,908.87 μm. Results were given in percentage relative to total sample. To achieve reliable results, each sample measurement was repeated 10 times and the average value was calculated. A *Sortable Silt mean* (SS) value (McCave et al., 2008; McCave et al., 1995) for estimating paleobottom current flow velocity was calculated by computing the weighted arithmetical means of the 10.29–60.52 μm grain size fractions for all samples as follows:

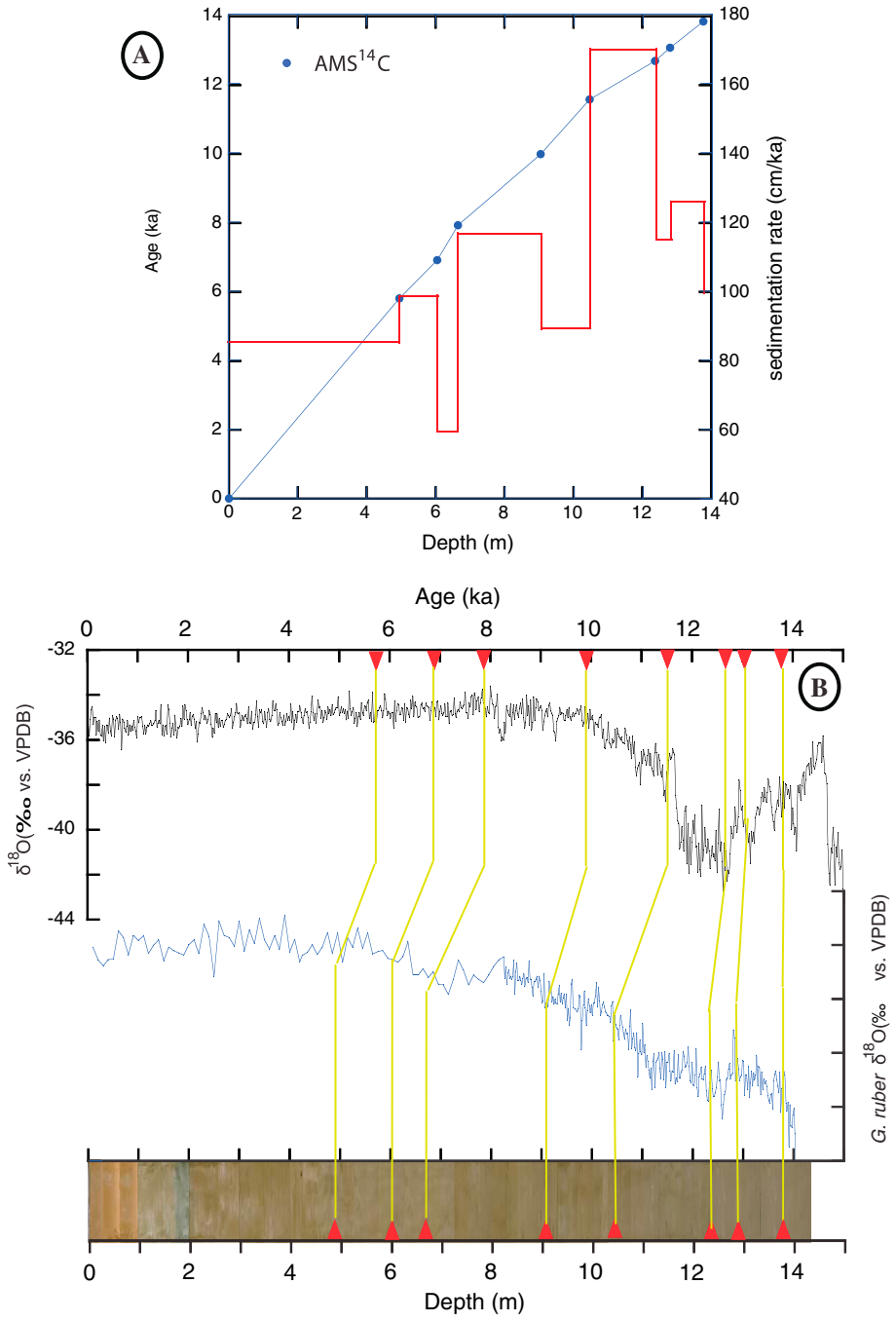

Figure 2. Age model of Core SO217-18517, based on eight accelerator mass spectrometry (AMS) ^{14}C dates (Table 1). (a) Depth/age plot. (b) Comparison of Northern Hemisphere ice core δ^{18}O (upper curve from Rasmussen et al., 2006) and SO217-18517 planktonic δ^{18}O signals (lower curve).

$$\overline{X} = \frac{\sum_{i=1}^{n} W_i X_i}{\sum_{i=1}^{n} W_i}$$

where $\overline{X}$ is the weighted arithmetical mean, W_i is the measured values, and X_i is the size classes.

2.9. Carbonate Content

Carbonate content was measured on dried and crushed bulk sediment using a carbonate bomb (Müller & Gastner, 1971). Samples were measured at 50 cm intervals throughout the core. The standard error of the carbonate bomb is ±1%.

Table 1
Pteropod and Planktonic Foraminiferal AMS ^{14}C Dates Used to Derive the Age Model in Core SO217-18517

No.	Type	Depth	Calendar age (year B.P.)	Description
1	Modern	0	0	Sediment-water interface
2	AMS^{14}C	495 cm (section 6, 70–71 cm)	5,809 ± 62	Pteropods. Conventional ages: 5,460 ± 35 years. Reservoir age: 400 years.
			5,742 ± 93	Reference: KIA 48504
3	AMS^{14}C	605 cm (section 7, 80–81 cm)	6,925 ± 52	Pteropods. Conventional ages: 6,470 ± 40 years. Reservoir age: 400 years.
			6,856 ± 103	Reference: KIA 50226
4	AMS^{14}C	665 cm (section 8, 40–41)	7,936 ± 41	Pteropods. Conventional ages: 7,505 ± 50 years. Reservoir age: 400 years.
			7,874 ± 87	Reference: KIA 49039
5	AMS^{14}C	905 cm (section 10, 80–82 cm)	9,993 ± 128	Planktonic foraminifers: *G. ruber*, *G. sacculifer*, and *G. trilobus*. Conventional ages:
			9,962 ± 139	9,270 ± 50 years. Reservoir age: 400 years. Reference: KIA 48505
6	AMS^{14}C	1,047 cm (section 12, 20–21 cm)	11,586 ± 150	Pteropods. Conventional ages: 10,455 ± 55 years. Reservoir age: 400 years.
			11,459 ± 180	Reference: KIA 48506
7	AMS^{14}C	1,237 cm (section 14, 10–11 cm)	12,704 ± 53	Pteropods. Conventional ages: 11,185 ± 55 years. Reservoir age: 400 years.
			12,622 ± 70	Reference: KIA 47981
8	AMS^{14}C	1,237 cm (section 14, 10–11 cm)	12,666 ± 52	Planktonic foraminifers: G. *ruber*, *G. sacculifer*, and *G. trilobus*. Conventional ages:
			12,471 ± 124	11,035 ± 55 years. Reservoir age: 400 years. Reference: KIA 47980
9	AMS^{14}C	1,281 cm (section 14, 54–55 cm)	13,087 ± 76	Pteropods. Conventional ages: 11,650 ± 70 years. Reservoir age: 400 years.
			13,035 ± 120	Reference: KIA 50227
10	AMS^{14}C	1,377 cm (section 15, 50–51 cm)	13,850 ± 72	Planktonic foraminifers: G. *ruber*, *G. sacculifer*, and *G. trilobus*. Conventional ages:
			13,835 ± 123	12,450 ± 70 years. Reservoir age: 400 years. Reference: KIA 49040

Note. Calendar ages in italics are derived from Calib 7.1.0 with calibration data set marine13.14c (Reimer et al., 2013) and a ΔR (local marine age correction) of 89 ± 70 years (Southon et al., 2002). The two AMS^{14}C dates for the depth of 1,237 cm (Nos. 7 and 8) represent replicate measurements using planktonic foraminifers and pteropods.

3. Results

3.1. Chronology

The planktonic $\delta^{18}O$ record from Core SO217-18517 indicates recovery of a complete succession from the Holocene down to Marine Isotope Stage 2 (Figure 2). AMS^{14}C dates are provided in Table 1 and Figure 2a.

The ends of the Bølling-Allerød (BA, 15–12.9 ka) and of the Younger Dryas (YD, 12.9–11.7 ka) are constrained by AMS ^{14}C dates 7 and 6 (Table 1), providing a robust estimate of sedimentation rate changes during these climate events. Average sedimentation rates are relatively constant at ~100 cm/kyr, except during the YD, when sedimentation rates reach 170 cm/kyr (Figure 2a).

3.2. X-Ray Fluorescence Derived Elemental Ratios

Log (Zr/Rb) and Log (K/Ti) exhibit an out of phase trend from the last deglaciation until the middle Holocene (14–7 ka) (Figure 3). Log (K/Ti) fluctuates between 0.23 and 0.35 during this interval with generally lower values during the deglaciation and a distinct decrease in the later part of the YD, leading to a pronounced minimum at the base of the Holocene (Figure 3f). The most prominent feature of the Log (K/Ti) curve is the sustained increase during the early Holocene, between ~11.5 and 10 ka. This increase is followed by a prolonged decrease to a minimum at ~7 ka, before a renewed increase between ~7 and 6 ka. After 6 ka, Log (K/Ti) becomes highly variable with numerous short terms, high-amplitude fluctuations, including a prominent minimum at ~1 kyr.

Log (Zr/Rb) is generally low during the deglaciation, except for a transient increase at the end of the BA (Figure 3b). The YD interval is marked by the lowest values (0.15 to 0.225). At the end of the YD, Log (Zr/Rb) increases rapidly from 0.2 to 0.3 between ~12.5 and 12 ka, leading the increase in Log (K/Ti) by at least 500 years. A prominent second rise in Log (Zr/Rb) from 0.23 to 0.35 occurs between ~9 and 7 ka, leading to a maximum at ~7 ka, followed by a consistent decline to the present.

The relative abundance of terrigenous material (Ti, Fe, Al, and K) with respect to carbonate (supporting information Figure S5) reflects a combination of river discharge of suspended material in the low-salinity plume off the Mahakam Delta and transport/redeposition processes within the Makassar Strait. Log (K/Ca) and Log (Al/Ca) show similar trends from the late deglaciation to the late Holocene (Figures 3d and 3e). The YD is marked by maxima in Log (K/Ca) and Log (Al/Ca) with values of −0.2 and −0.5, respectively. A second, less pronounced peak occurs at 9 ka with values of −0.5 and −1.1, respectively. During the remaining part of the

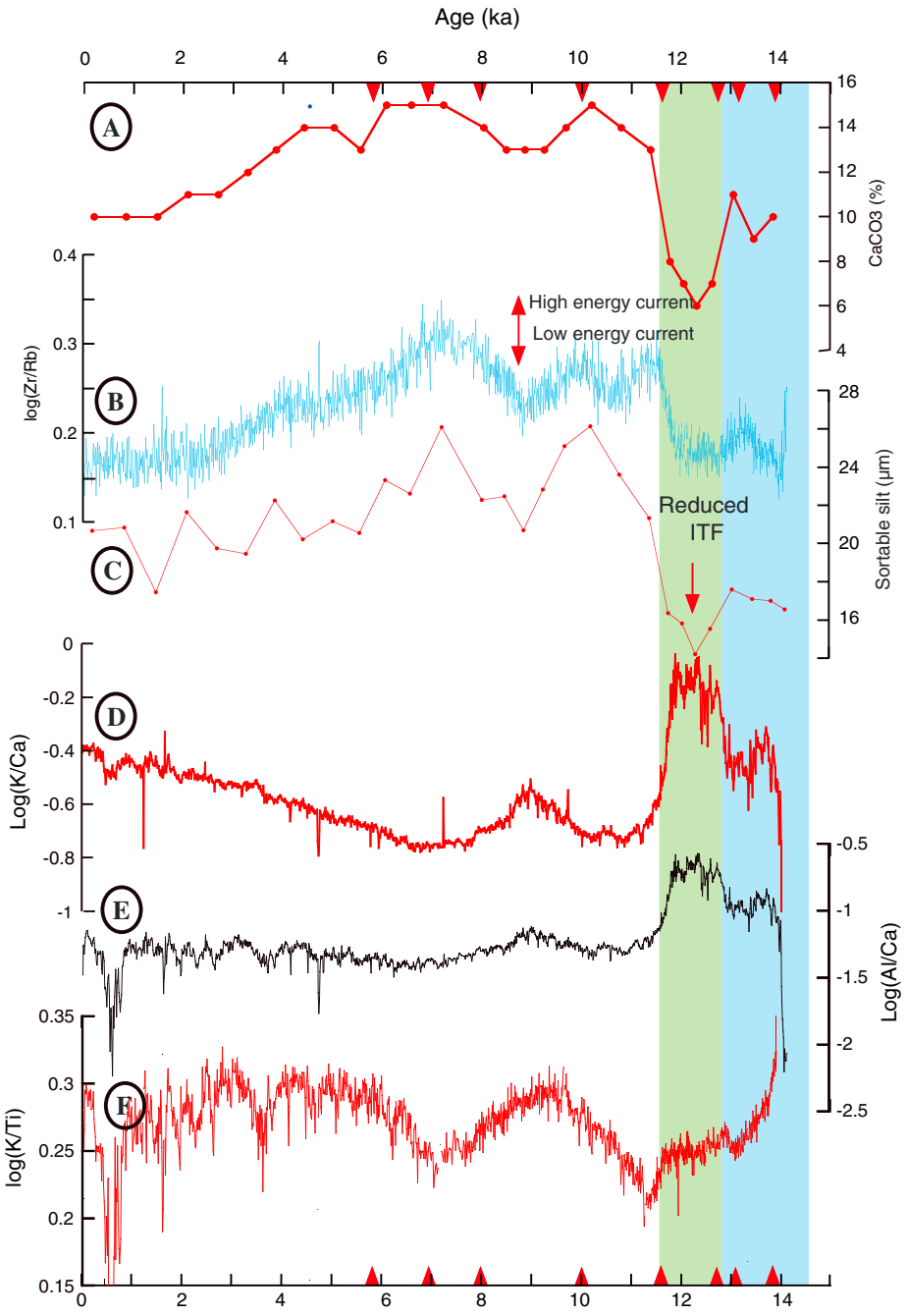

Figure 3. Comparison of sediment characteristics used for paleocurrent reconstruction in Core SO217-18517. (a) Carbonate bomb measurements at 50 cm intervals; (b) Normalized ratio of Zr/Rb from X-ray fluorescence measurements at 1 cm intervals; (c) Grain size measurement at 50 cm intervals; (d) Normalized log (K/Ca) at 1 cm intervals; (e) Normalized ratio of log (Al/Ca) at 1 cm intervals; and (f) Normalized ratio of K/Ti from X-ray fluorescence measurements at 1 cm intervals. Green shading marks Younger Dryas; blue shading marks Bølling-Allerød.

Holocene, Log (K/Ca) is characterized by an increasing trend from −0.8 and −0.4. In contrast, Log Al/Ca fluctuates around a mean of −1.2 between 8 and 1 ka and displays an abrupt decline at ~ 1 ka.

3.3. Planktonic $\delta^{18}O$, Sea Surface Temperature, and $\delta^{18}O_{sw}$ Reconstructions

3.3.1. *Globigerinoides ruber* $\delta^{18}O$ Variability

Surface $\delta^{18}O$ in Core SO217-18517 shows an overall deglacial decrease from ~−1.4 to ~−3.0‰ (Figure 4a). In the oldest part of the record, corresponding to the BA plateau between ~14 and 12.9 ka, $\delta^{18}O$ exhibits a stepwise decrease from −1.4 to −1.9‰. This is followed by a brief increase between 12.9 and 12.5 ka and

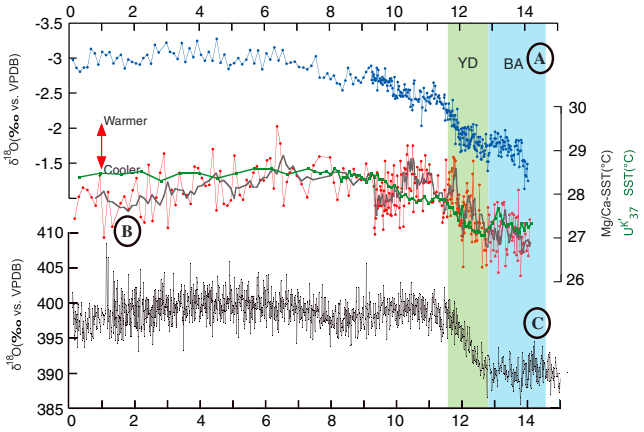

Figure 4. Paleotemperature and stable isotope records from Core SO217-18517 combined with Southern Hemisphere ice core record. (a) $\delta^{18}O$ of *Globigerinoides ruber* at 2 cm intervals during deglaciation and at 10 cm intervals during Holocene. (b) *Globigerinoides ruber* Mg/Ca-derived temperature in same resolution as $\delta^{18}O$; 5-point running average of Mg/Ca shown in gray; alkenone U^{k}_{37} in same sample spacing as $\delta^{18}O$ in green. (c) Southern Hemisphere ice core $\delta^{18}O$ record (EPICA Community Members, 2006). Green shading marks Younger Dryas; blue shading marks Bølling-Allerød.

a second plateau with $\delta^{18}O$ in the range of −2‰ from ~12.5 to 12.0 ka, which correspond to the YD cooling interval (12.9–11.7 ka) in Northern Hemisphere high latitudes. $\delta^{18}O$ values decrease rapidly from −2 to −2.9‰ between ~12 and 9 ka and fluctuate between −2.8 and −3.3‰ from ~9 to 0 ka, with lowest values in the range of −3.3‰ between ~5 and 3 ka. However, the low sample resolution and the long interpolation distance between the uppermost AMS ^{14}C date at 5809 ± 62 ka and the present sea floor age do not allow a precise delineation of this middle to late Holocene $\delta^{18}O$ minimum. A distinct $\delta^{18}O$ increase to −2.45‰ in the early part of this interval is tentatively attributed to a cooling event at ~8.2 ka.

3.3.2. Mg/Ca Temperature Reconstruction

Mg/Ca in Core SO217-18517 exhibit an average of 4.66 mmol/mol, corresponding to a mean of 27.8°C in SST during the deglacial to late Holocene period. The total amplitude of Mg/Ca derived SST ranges from 26.1 to 29.5°C (Figure 4b). The most prominent feature of the record is the overall increase of ~2°C between ~14 and 10.5 ka, followed by a rapid decline by almost 1°C between 10.5 and 9.5 ka, resulting in a short-lived cool period at ~9.5 ka with average temperatures of ~27.5°C. Holocene SST fluctuates at ~28°C after 9.5 ka with a transient maximum of ~29.5°C at ~6 ka and exhibits an overall cooling trend in the late Holocene.

3.3.3. $U^{K'}_{37}$ Temperature Reconstruction

Alkenone-based SST in Core SO217-18517 exhibits a range of 27.1 to 28.6°C during the deglaciation and Holocene (Figure 4b). From the late deglaciation to earliest Holocene (~14–9 ka), temperatures increase by ~1.5°C, then remain steady at ~28.5°C over the last 9 ka. A marked cooling down to 27°C occurred at ~12.5 ka during the YD, following the BA temperature maximum of 27.8° at ~13 ka.

3.3.4. $\delta^{18}O_{sw}$ Variability

During the deglaciation, $\delta^{18}O_{sw}$ (corrected for ice volume) fluctuates between −0.6 and 0.4‰ in Core SO217-18517 (Figure 5b). During the BA, $\delta^{18}O_{sw}$ decreases to −0.2‰ followed by an increase to maximum values of 0.2‰ during the YD. A stepwise decrease in $\delta^{18}O_{sw}$ occurs between the late YD and early Holocene with a minimum of −0.5‰ at ~9.5 ka, followed by a rapid increase to ~−0.1‰ at ~9 ka. The Holocene is characterized by a steady decrease from −0.1 to −0.5‰ between ~9 and 5 ka and a slightly increasing trend from ~5 to 0 ka.

3.4. Grain Size Variability

Estimates of paleobottom current intensity were obtained from sortable silt mean values in Core SO217-18517 (Figure 3c). Finer grain sizes generally occur during the late deglaciation. A distinct minimum in grain size is reached at 12.3 ka in the middle of the YD with a mean sortable silt value of 14.2 μm, followed by a slow increase to ~16 μm and a rapid increase by ~10 μm from the end of the YD to the early Holocene (~10.3 ka), where a first maximum of ~26 μm occurs. Mean grain sizes then decrease to a minimum at ~9 ka before a second increase to a maximum of ~26 μm at ~7.5 ka. Decreasing grain sizes to a minimum of 14.8 μm at ~2 ka characterize the middle and late Holocene. Overall, the sortable silt records parallel the grain density/size proxy records, based on Log (Zr/Rb) (Figures 3b and S6a). Both records show a consistent trend toward finer grain sizes during the YD, followed by a rapid increase toward a double peaked maximum during the early Holocene and a slow, but steady decline during the middle to late Holocene.

3.5. Carbonate Content

Carbonate content varies between 6 and 15% over the past 14 ka in Core SO217-18517 (Figure 3a) and is closely reflected in the XRF scanner derived Ca Area counts (supporting information Figure S6b). The carbonate content parallels the sortable silt and Log(Zr/Rb) curves. Lowest carbonate percentages occur during the YD. Carbonate content values fluctuate between 10 and 15% during the Holocene, with highest values in the early and middle Holocene and a decreasing trend toward the Recent.

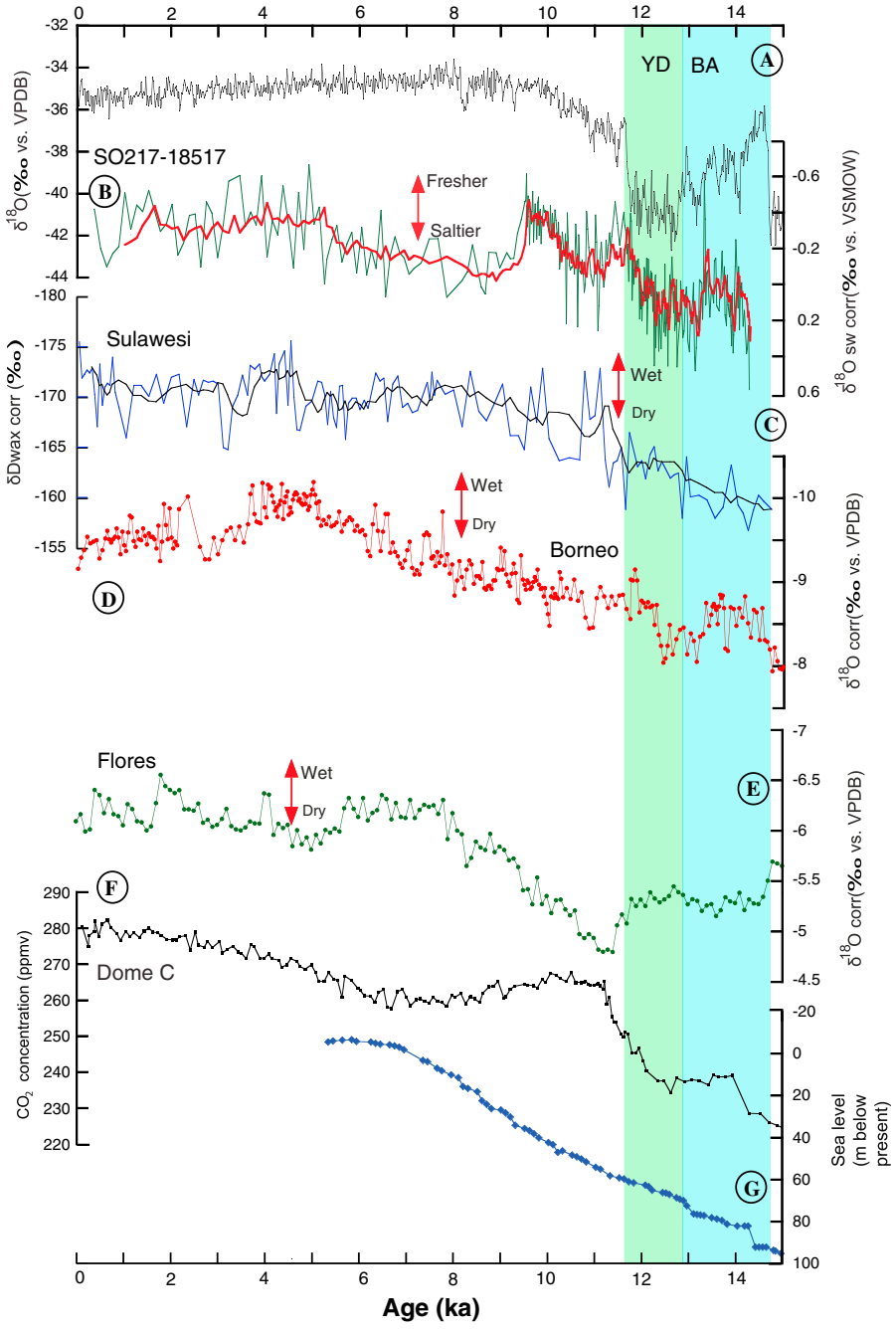

Figure 5. Comparison of regional precipitation proxy data from the Indonesian region with high latitude climate records. (a) Northern Hemisphere ice core $\delta^{18}O$ record (Rasmussen et al., 2006). (b) $\delta^{18}O_{sw}$ reconstruction, based on paired $\delta^{18}O$ and Mg/Ca-derived temperature data; 5-point running average of $\delta^{18}O_{sw}$ shown in red. (c) δD_{wax} record from Core 70GGC off Sulawesi (Tierney et al., 2012); 5-point running average shown in black. (d) Stalagmite records from northern Borneo (Carolin et al., 2013 after Partin et al., 2007). (e) Stalagmite records from Flores (Ayliffe et al., 2013). (f) Antarctic Ice Core (Dome Concordia) pCO_2 record (Monnin et al., 2001). (g) Sea level reconstruction (Sarnthein et al., 2011). Green shading marks Younger Dryas; blue shading marks Bølling-Allerød.

4. Discussion

4.1. ITF Variability and Mahakam Delta Discharge

4.1.1. Slowdown of the ITF During the YD

The lowest carbonate concentrations and highest accumulation of terrigenous material at Site SO217-18517 occurred during the last deglaciation and especially during the YD (Figure 3a). However, complex changes in provenance, delta configuration, and associated discharge patterns as well as resuspension/winnowing

processes at the site of deposition need to be considered when interpreting fluctuations in terrigenous accumulation as a proxy for riverine runoff difficult. We therefore use two additional proxies for bottom current speed, based on grain size (sortable silt) and grain density (Log (Zr/Rb)), to assess the influence of resuspension and winnowing on sediment accumulation at Site SO217-18517. We also use the ratios of K to other terrigenous elements as an indicator of sediment provenance (Diekmann et al., 2008; Eisma & van der Marel, 1971; Kujau et al., 2010; Potter et al., 2005; Rothwell & Croudace, 2015; Tian et al., 2011).

Paleocurrent indicators (sortable silt and Log (Zr/Rb)) indicate a dramatic decrease in bottom current velocities at ~640 m paleowater depth along the western margin of the Makassar Strait during the YD (Figures 3b and 3c). The following increase in grain size and density at the end of the YD is paralleled by a decrease in Log (Al/Ca) and Log (K/Ca), interpreted as reduced accumulation of clay minerals due to winnowing of the <2 μm fine fraction by intensified bottom currents. Today, the maximum thermocline flow occurs during boreal summer (August–September), when the SW trade winds are strongest and substantially reduce or even reverse the ITF southward surface flow in the Makassar Strait (Gingele et al., 2001; Gordon et al., 2008). While a strong surface flow transports clay minerals and other fine grained particles from Borneo southward along the Makassar Strait (Eisma et al., 1989; Gingele et al., 2001; Kuhnt et al., 2004), a strong thermocline flow may resuspend illite and kaolinite from the <2 μm fraction, which is the main source of K and Al in the sediment of Core SO217-18517. Thus, minimum values in the sortable silt record (Figure 3c) and an increase in Log (K/Ca) and Log (Al/Ca) (Figures 3d and 3e) indicate a marked slowdown of the deep thermocline ITF in the Makassar Strait during the YD. This weaker thermocline flow would reduce winnowing and resuspension at the location of Core SO217-18517, leading to an increase in the accumulation of clay minerals and elevated sedimentation rates between the age tie points at 12,704 ± 53 and 11,586 ± 150 years B.P. (Figure 2a and supporting information Figure S7).

4.1.2. Early Holocene Increase in Mahakam Delta Discharge

Deviation of K from other siliciclastic elements and low correlation of K to Ti ($r^2 = 0.56$) and Fe ($r^2 = 0.52$) has been used in a study of sediment discharge from the Mississippi into the Gulf of Mexico to discriminate between different terrigenous sources for K, which is common in illite-rich clays (>2% K in illite-rich clays and 6% in pure illite), and other terrigenous elements (Al, Si, Ti, and Fe) that dominate in kaolinite-rich clays from areas exposed to intense tropical weathering (Kujau et al., 2010). Characteristically, K weight percentages in surface samples from the Mahakam River range between 1.3 and 1.6% in the bulk sediment (<63 μm) but reach 2.4–2.6% in the clay fraction (<2 μm) (Liu et al., 2012). In our records, the correlation of K to Ti, Al, and Fe ($r^2 = 0.92$, $r^2 = 0.91$, and $r^2 = 0.76$, respectively, supporting information Figure S5) is higher than offshore the Mississippi Delta, indicating a more coherent source of the sediment discharge. However, the downcore variability in Log(K/Ti) (Figure 3f) differs significantly from the grain size/current proxies (Figures 3b and 3c). Low Log(K/Ti) values from K-depleted (illite-poor) sediments dominate until ~11.5 ka, while sortable silt and grain size/bottom current indicator Log(Zr/Rb) increase substantially after ~12 ka. We interpret the marked increase in Log(K/Ti) between ~11.5 and 9.5 ka as the intensification of runoff from the Mahakam Delta. Decreases in Log(K/Ti) at ~7 ka and between ~4 and 1 ka with several spikes of unusually K-depleted sediments were probably caused by changes in sediment deposition dynamics within the Mahakam Delta. The delta prograded by ~60 km during the late Holocene slow rise in local sea level over the past 5 kyr (Storms et al., 2005). Thus, the progradational delta system developed highly variable distributary and depositional patterns that likely caused substantial changes in the flux and characteristics of terrigenous sedimentation. However, the consistent trend in Log(Zr/Rb) over this period provides further evidence that this parameter is reflecting ITF flow within the Makassar Strait rather than sediment dynamics within the Mahakam Delta.

4.2. Changes in Seasonality Across the YD

The Mg/Ca derived SST record reveals low variability through the last deglaciation, whereas *G. ruber* $\delta^{18}O$ increases at the beginning of the YD (Figure 4a). Moreover, alkenone-based temperature estimates show a cooling to minimum values of 27°C in the early part of the YD (Figure 4b), whereas Mg/Ca derived SST indicates a consistent warming during the YD period (Figure 4b). A discrepancy between alkenone and Mg/Ca-based temperature estimates in the South China Sea during the last deglaciation was attributed to different seasonalities of the proxies used for temperature reconstructions (Steinke et al., 2008).

Today, tropical $U^{K'}_{37}$ temperatures are linked to the seasonal productivity of coccolithophorids, which thrive in periods of intensified upwelling and upper ocean mixing during the boreal winter monsoon and develop

intense blooms in early spring (Chen et al., 2007; Harada et al., 2001). In contrast, modern tropical Mg/Ca-derived SST generally reflects boreal summer temperatures (Timmermann et al., 2014; Wang et al., 2013). A strong seasonality in YD temperature reconstructions may be related to an intensified cross equatorial atmospheric flow. An extreme southerly mean position of the ITCZ during the YD (e.g., Kuhnt et al., 2015), associated with flooding of the vast Sunda shelf landmass (Hanebuth et al., 2000), probably promoted a vigorous cross equatorial flow from the Northern Hemisphere during the boreal winter monsoon. This cool air mass would explain the low $U^{K'}_{37}$-derived SST (Figure 4b). In contrast, Mg/Ca-derived SST (Figure 4b), which closely follows Southern Hemisphere $\delta^{18}O$ ice core records (Figure 4c), may have been mainly influenced by southeasterly trade winds during austral winter, as proposed for records from offshore East Africa (Wang et al., 2013). Changes in local insolation may have additionally contributed to these seasonally biased temperature records. Boreal summer (June–July) insolation at the latitude of the coring site (1°S) was consistently higher than today, while winter (December) insolation was significantly lower (supporting information Figure S3).

4.3. Variability in Convective Precipitation

Today, the convective precipitation over East Borneo is sensitive to annual changes in the position of the ITCZ (Figure 1). In the Samarinda area, which is closest to our coring site, a double maximum in precipitation occurs in December and April, when the ITCZ is on its annual southward and northward swings at the beginning and end of the austral summer monsoon. The driest season occurs in June to October, associated with the northern position of the ITCZ. Precipitation is also reduced during the peak Australian summer monsoon in January–March, when the ITCZ is over northern Australia. Today, peaks in the Mahakam River discharge, which has a yearly average rate of $>$8,000 m^3/s (Sassi et al., 2011), occur in January and April following the regional precipitation maxima. Most of the fluvial discharge is deposited in lakes within the catchment area and on the Samarinda alluvial plain (supporting information Figure S1). A recent quantitative analysis of depositional processes in the Mahakam Delta showed that 79% of the fine-grained sediment discharge is transported through the southern distributaries of the Mahakam Delta (Lambiase, 2013), which are located close to our coring site. Conductivity, temperature and depth measurements during R/V *Sonne* cruise SO-217 indicated that low surface salinities of $<$33.5 psu prevail even during the dry season in August due to the proximity of the Mahakam Delta (Kuhnt et al., 2011). This low salinity plume (supporting information Figure S1) spreads along 400 km to the southeast within the Makassar Strait and transports suspended matter in the order of 0.3 to 0.5 mg/dm^3 (Eisma et al., 1989). Sediment accumulation and salinity changes at Site SO217-18517 are, thus, closely related to water and sediment discharge from the southern distributaries of the Mahakam Delta.

Deglacial records of convective precipitation over northern Borneo indicated that dry conditions in the WPWP accompanied cooling events in the northern high latitudes (Carolin et al., 2013; Meckler et al., 2012; Partin et al., 2007) (Figures 5b and 5c). These cooling trends were tentatively related to southward shifts of the ITCZ during Northern Hemisphere cooling. Denton et al. (2010) proposed a linkage between increased temperature seasonality and winter sea ice in the Northern Hemisphere with weakening of the Asian summer monsoon during the YD and H1. Since these intervals coincide with increased precipitation in southern Indonesia (Griffiths et al., 2009) (Figure 5e) and Australia (Kuhnt et al., 2015; Muller et al., 2008), these authors proposed that southward swings of the ITCZ exerted a major control on precipitation patterns over most of Indonesia and NW Australia. However, changes in the intensity of the tropical convection (Tierney et al., 2010), Walker circulation, El Niño–Southern Oscillation system (Levi & Elderfield, 2007; Stott et al., 2004), and sea level (Griffiths et al., 2009; Partin et al., 2007) may have strongly modified the influence of ITCZ swings on precipitation patterns over the Australian-Indonesian region during the last deglaciation.

Our reconstructed $\delta^{18}O_{sw}$ at Site SO217-18517 (Figure 5b) shows an increase during the BA and a decrease during the YD, which is in agreement with speleothem $\delta^{18}O$ records from northeastern Borneo (Carolin et al., 2013; Partin et al., 2007; Figure 5d). However, this is in contrast to the cave records of Flores and the δD_{wax} records offshore SW Sulawesi, which exhibit no significant difference between the BA and YD (Griffiths et al., 2009, Griffiths, Drysdale, Gagan, et al., 2010, Griffiths, Drysdale,Vonhof, et al., 2010; Figure 5e) or show a decreasing trend of δD_{wax} from the BA to the YD (Tierney et al., 2012; Figure 5c). A possible controlling mechanism for these latitudinal differences may be a southward shift of the ITCZ and tropical rain belt during the YD, also detected in XRF scanner-derived terrigenous river runoff patterns from NW Australia

(Kuhnt et al., 2015). Wet BA and dry YD conditions, as in East Borneo and south of Java (Mohtadi et al., 2011), were associated with intense cross-equatorial moisture transport from the Northern Hemisphere (Mohtadi et al., 2011). The deglacial sea level rise (Meltwater Pulse 1A at 14.3 ka, Hanebuth et al., 2000) and associated flooding of large parts of Sundaland may have additionally led to intensification of the Indonesian-Australian Monsoon during the BA (Griffiths et al., 2009; Partin et al., 2007). In contrast, the abrupt $\delta^{18}O_{sw}$ increase, detected at ~9 ka in Core SO217-18517, is not apparent in reconstructed precipitation patterns from NE Borneo (Carolin et al., 2013; Partin et al., 2007). This may reflect local, sea level-related dynamics of the Mahakam River discharge and its associated low-salinity plume within the Makassar Strait.

5. Conclusion

Paleocurrent indicators (sortable silt and XRF scanner-derived Log (Zr/Rb)) indicate a dramatic decrease in bottom current velocities at ~640 m paleowater depth along the western margin of the Makassar Strait during the YD. Decreased winnowing in combination with increased sedimentation rates provides robust evidence for a weakening of the thermocline ITF flow during the YD. The $\delta^{18}O$ of seawater offshore the Mahakam Delta decreases during the BA and increases during the YD, indicating a dry YD in the catchment area of the Mahakam River in agreement with speleothem $\delta^{18}O$ records from NE Borneo (Carolin et al., 2013; Partin et al., 2007). The contrast with more southerly $\delta^{18}O$ cave records and δD_{wax} data, which exhibit no significant difference or display a decreasing trend from the BA to YD (Griffiths et al., 2009. Griffiths, Drysdale, Gagan, et al., 2010, Griffiths, Drysdale,Vonhof, et al., 2010, Tierney et al., 2012) is likely due to a southward shift of the ITCZ and tropical rain belt during the YD. An extreme southerly mean position of the ITCZ during the YD would have promoted a vigorous cross equatorial flow from the Northern Hemisphere during the boreal winter monsoon.

Acknowledgments

We acknowledge the Captain and the crew of R/V *Sonne* for all their efforts and support during Sonne-217 MAJA Cruise from July to mid-August 2011 in the Indonesian seas. We are grateful to Dieter Garbe-Schönberg and Ulrike Westernstroer for help with the X-Ray Fluorescence Scanner and ICP-OES Mg/Ca measurements and to Dörte Mikschl for technical assistance during sampling and sample preparation. We thank Nils Andersen and Matthias Hüls (Leibniz Laboratory Kiel) for stable isotope and ^{14}C measurements and Marcus Regenberg and Daniel Unverricht for help with Mg/Ca paleothermometry and sortable silt grain size analyses. We also thank Sri Yudawati Cahyarini at the Indonesian Institute of Sciences for discussion. We gratefully acknowledge the Deutsche Forschungsgemeinschaft (grant KU649/29-1) for funding this research and the Germany Ministry for Education and Science (BMBF, grant SO-217, and MAJA, 03G0217A) for funding the Sonne-217 Cruise. Data presented in this paper are archived at www.pangaea.de.

References

Aldrian, E., & Susanto, R. D. (2003). Identification of three dominant rainfall regions within Indonesia and their relationship to sea surface temperature. *International Journal of Climatology*, *23*(12), 1435–1452. https://doi.org/10.1002/joc.950

Anand, P., Elderfield, H., & Conte, M. H. (2003). Calibration of Mg/Ca thermometry in planktonic foraminifera from a sediment trap time series. *Paleoceanography 18*(2), 1050. https://doi.org/10.1029/2002PA000846

Andrews, J. T., Jennings, A. E., Kerwin, M., Kirby, M., Manley, W., & Miller, G. H. (1995). A Heinrich-like event, H-0 (DC-0): Source(s) for detrital carbonate in the North Atlantic during the Younger Dryas chronozone. *Paleoceanography*, *10*(5), 943–952. https://doi.org/10.1029/95PA01426

Ayliffe, L. K., Gagan, M. K., Zhao, J., Drysdale, R. N., Hellstrom, J. C., Hantoro, W. S., … Suwargadi, B. W. (2013). Rapid interhemispheric climate links via the Australasian monsoon during the last deglaciation. *Nature Communications*, *4*, 2908–2906. https://doi.org/10.1038/ncomms3908

Barker, S., Greaves, M., & Elderfield, H. (2003). A study of cleaning procedures used for foraminiferal Mg/Ca paleothermometry. *Geochemistry, Geophysics, Geosystems*, *49*, 8407. https://doi.org/10.1029/2003GC000559

Bemis, B. E., Spero, H. J., Bijma, J., & Lea, D. W. (1998). Reevaluation of the oxygen isotopic composition of planktonic foraminifera: Experimental results and revised paleotemperature equations. *Paleoceanography*, *13*(2), 150–160. https://doi.org/10.1029/98PA00070

Bolliet, T., Holbourn, A., Kuhnt, W., Laj, C., Kissel, C., Beaufort, L., … Garbe-Schönberg, D. (2011). Mindanao dome variability over the last 160 kyr: Episodic glacial cooling of the West Pacific warm pool. *Paleoceanography*, *26*, PA1208. https://doi.org/10.1029/2010PA001966

Boyle, E. A., & Keigwin, L. (1987). North Atlantic thermohaline circulation during the past 20,000 years linked to high-latitude surface temperature. *Nature*, *330*(6143), 35–40.

Broecker, W. S. (2003). Does the trigger for abrupt climate change reside in the ocean or in the atmosphere? *Science*, *300*(5625), 1519–1522. https://doi.org/10.1126/science.1083797

Carolin, S. A., Cobb, K. M., Adkins, J. F., Clark, B., Conroy, J. L., Malang, J., & Tuen, A. A. (2013). Varied response of western Pacific the hydrology to climate forcings over the last glacial period. *Science*, *340*(6140), 1564–1566. https://doi.org/10.1126/science.1233797

Chen, Y. L., Chen, H. Y., & Chung, C. W. (2007). Seasonal variability of coccolithophore abundance and assemblage in the northern South China Sea. *Deep-Sea Research Part II: Topical Studies in Oceanography*, *54*(14–15), 1617–1633. https://doi.org/10.1016/j.dsr2.2007.05.005

Conte, M. H., Sicre, M. A., Rühlemann, C., Weber, J. C., Schulte, S., Schulz-Bull, D., & Blanz, T. (2006). Global temperature calibration of the alkenone unsaturation index ($U^{K'}37$) in surface waters and comparison with surface sediments. *Geochemistry, Geophysics, Geosystems*, *7*, Q02005. https://doi.org/10.1029/2005GC001054(2)

De Deckker, P., Tapper, N. J., & Van der Kaars, S. (2003). The status of the indo-Pacific warm pool and adjacent land at the last glacial maximum. *Global and Planetary Change*, *35*(1-2), 25–35. https://doi.org/10.1016/S0921-8181(02)00089-9

Dekov, V. M., Van Put, A., Eisma, D., & Van Grieken, R. (1999). Single particle analysis of suspended matter in the Makasar Strait and Flores Sea with particular reference to tin-bearing particles. *Journal of Sea Research*, *41*(1-2), 35–53.

Denton, G. H., Anderson, R. F., Toggweiler, J. R., Edwards, R. L., Schaefer, J. M., & Putnam, A. E. (2010). The last glacial termination. *Science*, *328*(5986), 1652–1656.

Diekmann, B., Hofmann, J., Henrich, R., Fütterer, D. K., Röhl, U., & Wei, K.-Y. (2008). Detrital sediment supply in the southern Okinawa trough and its relation to sea-level and Kuroshio dynamics during the late quaternary. *Marine Geology*, *255*(1-2), 83–95.

DiNezio, P. N., Clement, A., Vecchi, G. A., Soden, B., Broccoli, A. J., Bliesner, B. L. O., & Braconnot, P. (2011). The response of the Walker circulation to Last Glacial Maximum forcing: Implications for detection in proxies. *Paleoceanography*, *26*, PA3217. https://doi.org/10.1029/2010PA002083

Dypvik, H., & Harris, N. B. (2001). Geochemical facies analysis of fine-grained siliciclastics using Th/U, Zr/Rb and (Zr+Rb)/Sr ratios. *Chemical Geology*, *181*(1-4), 131–146.

Eisma, D., Kalf, J., Karmini, M., Mook, W. G., Van Put, A., Bernard, P., & Van Grieken, R. V. (1989). Dispersal suspended matter in Makassar Strait and Flores Basin. *Netherlands Journal of Sea Research*, *24*(4), 383–398. https://doi.org/10.1016/0077-7579(89)90116-6

Eisma, D., & van der Marel, H. W. (1971). Marine muds along the Guyana coast and their origin from the Amazon Basin. *Contributions to Mineralogy and Petrology*, *31*(4), 321–334.

EPICA Community Members (2006). One-to-one coupling of glacial climate variability in Greenland and Antarctica. *Nature*, *444*(7116), 195–198. https://doi.org/10.1038/nature05301

Fairbanks, R. G., Evans, M. N., Rubenstone, J. L., Mortlock, R. A., Broad, K., Moore, M. D., & Charles, C. D. (1997). Evaluating climate indices and their geochemical proxies measured in corals. *Coral Reefs*, *16*(5), S93–S100. https://doi.org/10.1007/s003380050245

Fairbanks, R. G., Mortlock, R. A., Chiu, T.-C., Cao, L., Kaplan, A., Guilderson, T. P., … Nadeau, M.-J. (2005). Radiocarbon calibration curve spanning 0 to 50,000 years BP based on paired 230Th/234U/238U and 14C dates on pristine corals. *Quaternary Science Reviews*, *24*(16-17), 1781–1796. https://doi.org/10.1016/j.quascirev.2005.04.007

Fraser, N., Kuhnt, W., Holbourn, A., Bolliet, T., Andersen, N., Blanz, T., & Beaufort, L. (2014). Precipitation variability within the West Pacific warm pool over the past 120 ka: Evidence from the Davao gulf, southern Philippines. *Paleoceanography*, *29*, 1094–1110. https://doi.org/10.1002/2013PA002599

Ganopolski, A., & Rahmstorf, S. (2001). Rapid changes of glacial climate simulated in a coupled climate model. *Nature*, *409*(6817), 153–158. https://doi.org/10.1038/35051500

Gingele, F. X., DeDeckker, P., & Hillenbrand, C. (2001). Clay mineral distribution in surface sediments between Indonesia and NW Australia—Source and transport by ocean currents. *Marine Geology*, *179*(3-4), 135–146. https://doi.org/10.1016/S0025-3227(01)00194-3

Gordon, A. (2005). Oceanography of the Indonesian seas. *Oceanography*, *18*(4), 13–13. https://doi.org/10.5670/oceanog.2005.18

Gordon, A. L., Susanto, R. D., Ffield, A., Huber, B. A., Pranowo, W., & Wirasantosa, S. (2008). Makassar Strait throughflow, 2004 to 2006. *Geophysical Research Letters*, *35*, L24605. https://doi.org/10.1029/2008GL036372

Griffiths, M. L., Drysdale, R. N., Gagan, M. K., Frisia, S., Zhao, J. xin, Ayliffe, L. K., … Suwargadi, B. W. (2010). Evidence for Holocene changes in Australian-Indonesian monsoon rainfall from stalagmite trace element and stable isotope ratios. *Earth and Planetary Science Letters*, *292*(1-2), 27–38. https://doi.org/10.1016/j.epsl.2010.01.002

Griffiths, M. L., Drysdale, R. N., Gagan, M. K., Zhao, J., Ayliffe, L. K., & Hellstrom, J. C. (2009). Increasing Australian–Indonesian monsoon rainfall linked to early Holocene sea-level rise. *Nature Geoscience*, *2*(9), 636–639. https://doi.org/10.1038/ngeo605

Griffiths, M. L., Drysdale, R. N., Vonhof, H. B., Gagan, M. K., Zhao, J., Ayliffe, L. K., … Suwargadi, B. W. (2010). Younger Dryas–Holocene temperature and rainfall history of southern Indonesia from δ18O in speleothem calcite and fluid inclusions. *Earth and Planetary Science Letters*, *295*(1–2), 30–36. https://doi.org/10.1016/j.epsl.2010.03.018

Hall, R., & Nichols, G. (2002). Cenozoic sedimentation and tectonics in Borneo: Climatic influences on orogenesis. *Geological Society of London, Special Publication*, *191*(1), 5–22. https://doi.org/10.1144/GSL.SP.2002.191.01.02

Hanebuth, T., Stattegger, K., & Grootes, P. M. (2000). Rapid flooding of the Sunda shelf: A late-Glacial Sea-level record. *Science*, *288*(5468), 1033–1035. https://doi.org/10.1126/science.288.5468.1033

Harada, N., Handa, N., Harada, K., & Matsuoka, H. (2001). Alkenones and particulate fluxes in sediment traps from the central equatorial Pacific. *Deep Sea Research Part I: Oceanographic Research Papers*, *48*(3), 891–907. https://doi.org/10.1016/S0967-0637(00)00077-7

Henry, L. G., McManus, J. F., Curry, W. B., Roberts, N. L., Piotrowski, A. M., & Keigwin, L. D. (2016). North Atlantic ocean circulation and abrupt climate change during the last glaciation. *Science*, *353*(6298), 470–474. https://doi.org/10.1126/science.aaf5529

Holbourn, A., Kuhnt, W., & Xu, J. (2011). Indonesian Throughflow variability during the last 140 ka: The Timor Sea outflow. *Geological Society, London, Special Publications*, *355*(1), 283–303. https://doi.org/10.1144/SP355.14

Kirby, M. E. (1998). Heinrich event-0 (DC-0) in sediment cores from the northwest Labrador Sea: Recording events in Cumberland sound? *Canadian Journal of Earth Sciences*, *35*(5), 510–519. https://doi.org/10.1139/e97-119

Kuhnt, W., Holbourn, A., Hall, R., Zuvela, M., & Käse, R. (2004). Neogene history of the Indonesian Throughflow. In P. Clift, et al. (Eds.), *Continent-ocean interactions within East Asian marginal seas* (pp. 1–22). Washington, DC: American Geophysical Union. https://doi.org/10.1029/149GM16

Kuhnt, W., Holbourn, A., Regenberg, M., Zuraida, R., Abiyoso, S., Aquit, M., … Xu, J. (2011). *Cruise report Sonne 217: Variability of the Indonesian throughflow within the Makassar-Java passage*. Kiel: Institute of Geosciences, Christian Albrechts-Universität zu Kiel.

Kuhnt, W., Holbourn, A., Xu, J., Opdyke, B., DeDeckker, P., & Mudelsee, M. (2015). Southern Hemisphere control on Australian monsoon variability during the late deglaciation and Holocene. *Nature Communications*, *6*, 5916–5917. https://doi.org/10.1038/ncomms6916

Kujau, A., Nürnberg, D., Zielhofer, C., Bahr, A., & Röhl, U. (2010). Mississippi River discharge over the last ~560,000 years—Indications from X-ray fluorescence core-scanning. *Palaeogeography, Palaeoclimatology, Palaeoecology*, *298*(3-4), 311–318. https://doi.org/10.1016/j.palaeo.2010.10.005

Kylander, M. E., Ampel, L., Wohlfarth, B., & Veres, D. (2011). High-resolution X-ray fluorescence core scanning analysis of les Echets (France) sedimentary sequence : New insights from chemical proxies. *Journal of Quaternary Science*, *26*(1), 109–117. https://doi.org/10.1002/jqs.1438

Lambiase, S. J. J. (2013). Sediment dynamics and depositional systems of the Mahakam Delta, Indonesia: Ongoing delta abandonment on a tide-dominated coast. *Journal of Sedimentary Research*, *83*(7), 503–521. https://doi.org/10.2110/jsr.2013.42

Levi, C., & Elderfield, H. (2007). Low-latitude hydrological cycle and rapid climate changes during the last deglaciation. *Geochemistry, Geophysics, Geosystems*, *8*, Q05N12. https://doi.org/10.1029/2006GC001514

Linsley, B. K., Rosenthal, Y., & Oppo, D. W. (2010). Holocene evolution of the Indonesian throughflow and the western Pacific warm pool. *Nature Geoscience*, *3*(8), 578–583. https://doi.org/10.1038/ngeo920

Liu, L., Jun, C., Yang, C., Junfeng, J., & Huayu, L. (2002). Variation of Zr/Rb ratios on the Loess Plateau of Central China during the last 130000 years and its implications for winter monsoon. *Chinese Science Bulletin*, *47*(15), 1298–1302. https://doi.org/10.1360/02tb9288

Liu, Z., Wang, H., Hantoro, W. S., Sathiamurthy, E., Colin, C., Zhao, Y., & Li, J. (2012). Climatic and tectonic controls on chemical weathering in tropical Southeast Asia (Malay peninsula, Borneo, and Sumatra). *Chemical Geology*, *291*, 1–12. https://doi.org/10.1016/j.chemgeo.2011.11.015

Lo Giudice Cappelli, E., Kuhnt, W., Holbourn, A., & Regenberg, M. (2016). Changes in Timor Strait hydrology and thermocline structure during the past 130 ka. *Palaeogeography, Palaeoclimatology, Palaeoecology*, *462*, 112–124. https://doi.org/10.1016/j.palaeo.2016.09.010

Martin, P. A., & Lea, D. W. (2002). A simple evaluation of cleaning procedures on fossil benthic foraminiferal Mg/Ca. *Geochemistry, Geophysics, Geosystems 3*(10), 1–8. https://doi.org/10.1029/2001GC000280

McCave, I. N., Carter, L., & Hall, I. R. (2008). Glacial–interglacial changes in water mass structure and flow in the SW Pacific Ocean. *Quaternary Science Reviews*, *27*(19-20), 1886–1908. https://doi.org/10.1016/j.quascirev.2008.07.010

McCave, I. N., Manighetti, B., & Robinson, S. G. (1995). Sortable silt and fine sediment size/composition slicing: Parameters for paleocurrent speed and paleoceanography. *Palaeoceanography*, *10*(3), 593–610. https://doi.org/10.1029/94PA03039

McManus, J. F., Francois, R., Gherardi, J.-M., Keigwin, L. D., & Brown-Leger, S. (2004). Collapse and rapid resumption of Atlantic meridional circulation linked to deglacial climate changes. *Nature*, *428*(6985), 834–837. https://doi.org/10.1038/nature02494

Meckler, A. N., Clarkson, M. O., Cobb, K. M., Sodemann, H., & Adkins, J. F. (2012). Interglacial hydroclimate in the tropical West Pacific through the Late Pleistocene. *Science*, *336*(6,086), 1301–1304. https://doi.org/10.1126/science.1218340

Milliman, J. D., & Farnsworth, K. L. (2011). *River discharge to the coastal ocean: A global synthesis*. Cambridge: Cambridge University Press. https://doi.org/10.1017/CBO9780511781247

Milliman, J. D., Farnsworth, K. L., & Albertin, C. S. (1999). Flux and fate of fluvial sediments leaving large islands in the East Indies. *Journal of Sea Research*, *41*(1-2), 97–107. https://doi.org/10.1016/S1385-1101(98)00040-9

Mohtadi, M., Oppo, D. W., Steinke, S., Stuut, J. W., Pol-Holz, R. D., Hebbeln, D., & Lückge, A. (2011). Glacial to Holocene swings of the Australian —Indonesian monsoon. *Nature Geoscience*, *4*(8), 540–544. https://doi.org/10.1038/ngeo1209

Monnin, E., Indermühle, A., Dällenbach, A., Flückiger, J., Stauffer, B., Stocker, T. F., … Barnola, J.-M. (2001). Atmospheric CO_2 concentrations over the last glacial termination. *Science*, *291*(5501), 112–114. https://doi.org/10.1126/science.291.5501.112

Morimoto, M., Abe, O., Kayanne, H., Kurita, N., Matsumoto, E., Yoshida, N., & Nin, E. (2002). Salinity records for the 1997–98 El Nino from Western Pacific corals. *Geophysical Research Letters*, *29*, 35-1–35-4. https://doi.org/10.1029/2001GL013521

Müller, G., & Gastner, M. (1971). *The 'Karbonat-Bombe', a simple device for the determination of carbonate content in sediment, soils, and other materials* (Vol. 10, pp. 466–469). Bremerhaven: Neues Jahrbuch für Mineralogie-Monatshefte.

Muller, J., Kylander, M., Wu, R. A. J., Weiss, D., Martinez-Cortizas, A., Legrande, A. N., … Jacobson, G. (2008). Possible evidence for wet Heinrich phases in tropical NE Australia: The Lynch's Crater deposit. *Quaternary Science Reviews*, *27*(5-6), 468–475. https://doi.org/10.1016/j.quascirev.2007.11.006

Muller, P. J., Kirst, G., Ruhland, G., von Storch, I., & Rosell-Mele, A. (1998). Calibration of the alkenone paleotemperature index $U_{37}^{K'}$ based on core-tops from the eastern South Atlantic and the global ocean (60°N-60°S). *Geochimica et Cosmochimica Acta*, *62*(10), 1757–1772. https://doi.org/10.1016/S0016-7037(98)00097-0

Partin, J. W., Cobb, K. M., Adkins, J. F., Clark, B., & Fernandez, D. P. (2007). Millennial-scale trends in west Pacific warm pool hydrology since the Last Glacial Maximum. *Nature*, *449*(7161), 452–455. https://doi.org/10.1038/nature06164

Piotrowski, A. M., Goldstein, S. L., Hemming, S. R., & Fairbanks, R. G. (2005). Temporal relationships of carbon cycling and ocean circulation at glacial boundaries. *Science*, *307*(5717), 1933–1938. https://doi.org/10.1126/science.1104883

Potter, P. E., Maynard, J. B., & Depetris, P. J. (2005). In P. E. Potter, J. B. Maynard, & P. J. Depetris (Eds.), *Provenance of mudstones. Like detective work—fingerprinting samples and profiling suspects* (pp. 157–174). Dordrecht, Netherlands: Springer.

Rasmussen, S. O., Andersen, K. K., Svensson, A. M., Steffensen, J. P., Vinther, B. M., Clausen, H. B., … Ruth, U. (2006). A new Greenland ice core chronology for the last glacial termination. *Journal of Geophysical Research*, *111*, D06102. https://doi.org/10.1029/2005JD006079

Reimer, P. J., Bard, E., Bayliss, A., Beck, J. W., Blackwell, P. G., Bronk Ramsey, C., … van der Plicht, J. (2013). IntCal13 and MARINE13 radiocarbon age calibration curves 0–50000 years cal BP. *Radiocarbon*, *55*(04), 1869–1887. https://doi.org/10.2458/azu_js_rc.55.16947

Richter, T. O., van der Gaast, S., Koster, B., Vaars, A., Gieles, R., de Stigter, H. C., … Van Weering, T. C. E. (2006). The Avaatech XRF core scanner: Technical description and applications to NE Atlantic sediments. *Geological Society, London, Special Publications*, *267*(1), 39–50. https://doi.org/10.1144/GSL.SP.2006.267.01.03

Rincón-Martínez, D., Lamy, F., Contreras, S., Leduc, G., Bard, E., Saukel, C., … Tiedemann, R. (2010). More humid interglacials in Ecuador during the past 500 kyr linked to latitudinal shifts of the equatorial front and the Intertropical convergence zone in the eastern tropical Pacific. *Paleoceanography*, *25*, PA2210. https://doi.org/10.1029/2009PA001868

Rothwell, R. G., & Croudace, I. W. (2015). Twenty years of XRF core scanning marine sediments: What do geocemical proxies tell us? In I. W. Croudace & R. G. Rothwell (Eds.), *Micro-XRF studies of sediment cores. Applications of a non-destructive tool for the environmental Sciences* (pp. 25–102). Dordrecht, Netherlands: Springer. https://doi.org/10.1007/978-94-017-9849-5_2

Saller, A. H., Noah, J. T., Ruzuar, A. P., & Schneider, R. (2004). Linked lowstand delta to basin-floor fan deposition, offshore Indonesia : An analog for deep-water reservoir systems. *AAPG Bulletin*, *88*(1), 21–46.

Sarnthein, M., Grootes, P. M., Holbourn, A., Kuhnt, W., & Kühn, H. (2011). Tropical warming in the Timor Sea led deglacial Antarctic warming and atmospheric CO_2 rise by more than 500 yr. *Earth and Planetary Science Letters*, *302*(3-4), 337–348. https://doi.org/10.1016/j.espl.2010.12.021

Sassi, M. G., Hoitink, A. J. F., Vermeulen, B., & Hidayat, H. (2011). Discharge estimation from H-ADCP measurements in a tidal river subject to sidewall effects and a mobile bed. *Water Resources Research*, *47*, W06504. https://doi.org/10.1029/2010WR009972

Schmidt, M. W., Spero, H. J., & Lea, D. W. (2004). Links between salinity variation in the Caribbean and North Atlantic thermohaline circulation. *Nature*, *428*(6979), 160–163. https://doi.org/10.1038/nature02346

Schneider, R. R., Price, B., Miiller, P. J., Kroon, D., & Alexander, I. (1997). Monsoon related variations in Zaire (Congo) sediment load and influence of fluvial silicate supply on marine productivity in the east equatorial Atlantic during the last 200, 000 years. *Paleoceanography*, *12*(3), 463–481. https://doi.org/10.1029/96PA03640

Schulte, P., & Speijer, R. P. (2009). Late Maastrichtian-Early Paleocene sea level and climate changes in the Antioch Church Core (Alabama, Gulf of Mexico margin, USA): A multi-proxy approach. *Geologica Acta*, *7*, 11–34. https://doi.org/10.1344/105.000000279

Sonzogni, C., Bard, E., Rostek, F., Dollfus, D., Rosell-Melé, A., & Eglinton, G. (1997). Temperature and salinity effects on alkenone ratios measured in surface sediments from the Indian Ocean. *Quaternary Research*, *47*(03), 344–355. https://doi.org/10.1006/qres.1997.1885

Southon, J., Kashgarian, M., Fontugne, M., Metiver, B., & Yim, W. W.-S. (2002). Marine reservoir corrections for the Indian Ocean and Southeast Asia. *Radiocarbon*, *44*(01), 167–180. https://doi.org/10.1017/S0033822200064778

Steinke, S., Kienast, M., Groeneveld, J., Lin, L., Chen, M., & Rendle-Bühring, R. (2008). Proxy dependence of the temporal pattern of deglacial warming in the tropical South China Sea : Toward resolving seasonality. *Quaternary Science Reviews*, *27*(7-8), 688–700. https://doi.org/10.1016/j.quascirev.2007.12.003

Storms, J. E. A., Hoogendoorn, R. M., Dam, R. A. C., Hoitink, A. J. F., & Kroonenberg, S. B. (2005). Late-Holocene evolution of the Mahakam delta, East Kalimantan, Indonesia. *Sedimentary Geology*, *180*(3-4), 149–166. https://doi.org/10.1016/j.sedgeo.2005.08.003

Stott, L., Cannariato, K., Thunell, R., Haug, G. H., Koutavas, A., & Lund, S. (2004). Decline of surface temperature and salinity in the western tropical Pacific Ocean in the Holocene epoch. *Nature*, *431*(7,004), 56–59. https://doi.org/10.1038/nature02903

Stouffer, R. J., Yin, J., Gregory, J. M., Dixon, K. W., Spelman, M. J., Hurlin, W., … Weber, S. L. (2006). Investigating the causes of the response of the thermohaline circulation to past and future climate changes. *Journal of Climate*, *19*(8), 1365–1387. https://doi.org/10.1175/JCLI3689.1

Tian, J., Xie, X., Ma, W., Jin, H., & Wang, P. (2011). X-ray fluorescence core scanning records of chemical weathering and monsoon evolution over the past 5 Myr in the southern South China Sea. *Palaeoceanography*, *26*, PA4202. https://doi.org/10.1029/2010PA002045

Tierney, J. E., Oppo, D. W., LeGrande, A. N., Huang, Y., Rosenthal, Y., & Linsley, B. K. (2012). The influence of Indian Ocean atmospheric circulation on warm pool hydroclimate during the Holocene epoch. *Journal of Geophysical Research*, *117*, D19108. https://doi.org/10.1029/2012JD018060

Tierney, J. E., Oppo, D. W., Rosenthal, Y., Russell, J. M., & Linsley, B. K. (2010). Coordinated hydrological regimes in the indo-Pacific region during the past two millennia. *Paleoceanography*, *25*, PA1102. https://doi.org/10.1029/2009PA001871

Timmermann, A., Sachs, J. P., & Timm, O. E. (2014). Assessing divergent SST behavior during the last 21 ka derived from alkenones and *G. ruber*-Mg/Ca in the equatorial Pacific. *Paleoceanography*, *29*, 680–696. https://doi.org/10.1002/2013PA002598

Villiers, S. De, Greaves, M., & Elderfield, H. (2002). An intensity ratio calibration method for the accurate determination of Mg/Ca and Sr/Ca of marine carbonates by ICP-AES. *Geochemistry, Geophysics, Geosystems*, *31*, 1001. https://doi.org/10.1029/2001GC000169

Visser, K., Thunell, R., & Stott, L. (2003). Magnitude and timing of temperature change in the Indo-Pacific warm pool during deglaciation. *Nature*, *421*, 3667–3670. https://doi.org/10.1038/nature01331.1

Waliser, D. E., & Gautier, C. (1993). A satellite-derived climatology of the ITCZ. *Journal of Climate*, *6*(11), 2162–2174. https://doi.org/10.1175/1520-0442(1993)006%3C2162:ASDCOT%3E2.0.CO;2

Wang, Y. V., Leduc, G., Regenberg, M., Andersen, N., Larsen, T., Blanz, T., & Schneider, R. R. (2013). Northern and southern hemisphere controls on seasonal sea surface temperatures in the Indian Ocean during the last deglaciation. *Paleoceanography*, *28*, 619–632. https://doi.org/10.1002/palo.20053

Weltje, G. J., & Tjallingii, R. (2008). Calibration of XRF core scanners for quantitative geochemical logging of sediment cores: Theory and application. *Earth and Planetary Science Letters*, *274*(3-4), 423–438. https://doi.org/10.1016/j.epsl.2008.07.054

Xie, P., & Arkin, P. A. (1997). Global precipitation: A 17-year monthly analysis based on gauge observations, satellite estimates, and numerical model outputs. *Bulletin of the American Meteorological Society*, *78*(11), 2539–2558.

Zuraida, R., Holbourn, A., Nurnberg, D., & Kuhnt, W. (2009). Evidence for Indonesian Throughflow slowdown during Heinrich events 3–5. *Paleoceanography*, *24*, PA2205. https://doi.org/10.1029/2008PA001653